Early Time Behavior in Reverberation Chambers and Its Effect on the Relationships Between Coherence Bandwidth, Chamber Decay Time, RMS Delay Spread, and the Chamber Buildup Time

Christopher L. Holloway, *Fellow, IEEE*, Haider A. Shah, Ryan J. Pirkl, *Member, IEEE*,
Kate A. Remley, *Senior Member, IEEE*, David A. Hill, *Life Fellow, IEEE*, and John Ladbury, *Member, IEEE*

Abstract—**Reverberation chambers are emerging as a test facility for testing wireless devices and for emulating different wireless multipath environments. The commonly used quantities for characterizing the chambers in wireless applications are 1) the chamber quality factor, 2) the chamber decay time (τ_{RC}), 3) the RMS delay spread of the time-domain chamber response τ_{rms}, and 4) the coherence bandwidth BW of the frequency-domain transfer function of the chamber. Analytic expressions that relate τ_{RC} and BW and the relationship between τ_{rms} and BW are given in the literature. However, these expressions neglect the early-time behavior of the chamber (the time before a chamber reaches a reverberant condition), and hence can give inconsistent results when one is analyzing experimental data. In this paper, we discuss the relationship between BW, τ_{RC}, and τ_{rms} for realistic chamber behaviors, and we present expressions for these relationships when one takes into account the early-time behavior of the reverberation chamber. This early-time behavior is crucial when one tries to assess and compare these different quantities in experimental data, and as we will see, the relationship between these quantities can be different for different chambers (i.e., different chamber sizes and loading conditions). The model presented here illustrates how the early-time behavior can affect these chamber characteristic quantities for loaded and unloaded chambers, and it also illustrates the problems that can occur when the early-time behavior is not considered.**

Index Terms—**Chamber decay time, coherence bandwidth, early-time behavior, reverberation chambers (RC), rms delay spread, wireless propagation environments.**

I. INTRODUCTION

A TYPICAL reverberation chamber (RC) is, at its most fundamental level, a shielded room (having metallic walls) with a complex-shaped metallic mode-stirring paddle (also called a stirrer or tuner) [1]. The paddle is designed to be non-symmetric and is used to create continuously changing boundary conditions for the electromagnetic fields in the chamber. The rotating paddle creates a statistical environment in the RC, and this statistical environment results in a unique test facility. Electromagnetic RC are becoming popular as alternative test facilities for both electromagnetic and electromagnetic compatibility measurements. Initially, RC were used as high field amplitude test facilities for electromagnetic interference and compatibility, and these chambers are currently used for a wide range of other measurement applications. These applications include: 1) radiation immunity of components and large systems, 2) radiated emissions, 3) shielding characterization of cables, connectors, and materials, 4) antenna measurements, 5) probe calibrations, 6) characterization of material properties, 7) absorption and heating properties of materials, 8) biological and biomedical effects, 9) testing of wireless devices, and 10) simulating various wireless multipath environments (see [1] and [2] for a list of papers on the different applications).

The characteristics of an RC for wireless applications are usually identified by one of the following four quantities: 1) the chamber quality factor Q, 2) the coherence bandwidth BW of the frequency-domain transfer function, 3) the RMS delay spread for the time-domain response of the chamber τ_{rms}, and 4) the chamber's decay time τ_{RC}. Typically, the relationships between these four quantities are derived assuming the energy density inside an RC behaves in a certain assumed or prescribed manner, i.e., it is assumed that the energy density may be represented by a single-exponential model. In order to understand this assumption, we need to discuss the behavior of the fields inside a chamber.

The behavior of the fields inside a RC can actually be divided into two distinct behaviors, an early-time (or buildup-time) behavior and a late-time behavior (see [3]–[5]). The late-time behavior of the chamber corresponds to the period in which the energy in the chamber is well developed into a reverberant field behavior, while the early-time behavior corresponds to the period during which the energy is building up to this reverberant condition. One way of thinking about the early-time behavior is that it is the time it takes the rays in the chamber to "learn" where the walls and paddle are in the chamber. Once the rays in the chamber have made several bounces, the late-time behavior of the chamber commences and the decaying single-exponential

model can be used to predict its behavior in the chamber [1] and [3].

While it has been shown throughout the years that a single exponential model represents the late-time energy density inside an RC, the early-time behavior in a chamber is not captured by this single-exponential representation. Since the commonly used relationships between the aforementioned four quantities are derived with a single-exponential model for the energy density in the RC, they do not hold in general. In fact, the ratio of the chamber decay-time τ_{RC} relative to the early-time behavior may be used to assess whether results from a single-exponential model are valid.

In this paper, we investigate how the early-time behavior of a chamber affects the relationship between the quantities used to characterize that chamber. We present a model that accounts for the buildup (or early-) time behavior of the chamber. With this model, we present new expressions relating τ_{RC}, τ_{rms}, and BW valid for both loaded and unloaded chambers. We also present an approximate expression for estimating the buildup time in the chamber and an expression for estimating the time when the reverberation behavior (represented by a single-exponential model) is reached. We show that these relationships (τ_{rc}, τ_{rms}, and BW) are a function of the buildup time behavior of the chamber, and hence are specific for a given RC. We will see that the ratio of the buildup time to decay time τ_{RC} governs when a single-exponential model for the chamber is adequate.

II. BACKGROUND

In this section, we 1) introduce the definitions and nomenclature used in this paper, 2) derive the basic relationships between the four quantities used to characterize the RC, and 3) discuss how these relationships fail when the early-time behavior is not taken into account. We start with the chamber quality factor Q, which is given by [1]

$$Q = \frac{\omega\, U}{P_d} \tag{1}$$

where U is the energy stored within the chamber, P_d is the power dissipated in the chamber, and $\omega = 2\pi f$ (where f is the frequency). A popular method of measuring Q in the chamber is discussed in [1] and [6] and is expressed as

$$Q = \frac{16\pi^2 V}{\lambda^3} \frac{\langle P_r \rangle}{P_t} = \frac{16\pi^2 V}{\lambda^3} \langle |S_{21}|^2 \rangle \tag{2}$$

where V is the volume of the chamber, λ is the free-space wavelength, $\langle P_r \rangle$ is the average received power, P_t is the transmitted power in the chamber, and $\langle\ \rangle$ represents an ensemble average. In the RC, the ensemble average is obtained from different measurement samples (ideally these samples are independent). The samples are obtained by different paddle (or stirring) positions, averaging of a "small" band of frequencies, and/or measuring the power at different locations in the chamber, among other methods. A discussion on how this averaging is done from scattering S parameter measurements is given in [6]. This power ratio is typically determined from the measured S_{21} between

two antennas placed in the chamber. The expression in (2) was derived assuming the antennas used in the measurement are ideal (matched with no losses) antennas with 100% antenna efficiency. As discussed in [7]–[9], this measured Q has losses associated with both the chamber and loss associated with the nonideal antennas. The ramifications of this in relating Q to τ_{RC} and/or τ_{rms} will be discussed in Section III-A.

The coherence bandwidth of the chamber may be obtained by calculating the auto-correlation $\mathcal{R}$ of the frequency-domain transfer function of the chamber [10]. This is possible because the chamber can be thought of as a radio-propagation channel, and the autocorrelation (and corresponding coherence bandwidth) of a radio channel is obtained from the frequency-domain transfer function of the channel [11] and [12]. Typically, the frequency-domain transfer function of the chamber is obtained by means of a vector network analyzer that measures the S-parameters between two antennas placed inside a chamber, see [6] for details. The transfer function is then given by S_{21}. Thus, $\mathcal{R}$ (for a stationary process) is obtained from

$$\mathcal{R}(f) = \int_{f_{\mathrm{start}}}^{f_{\mathrm{stop}}} S_{21_n}(g)\, S_{21_n}^*(g - f)\, dg \tag{3}$$

where $*$ denotes the complex conjugate of S_{21_n}, and the subscript n corresponds to different samples obtained from paddle stirring, frequency stirring, and/or position stirring. The ensemble average (taken over the n samples) autocorrelation $\mathcal{R}_{\mathrm{avg}}$ for the different samples is given by

$$\mathcal{R}_{\mathrm{avg}} = \langle \mathcal{R}(f) \rangle. \tag{4}$$

While there is no rigid rule used to determine the coherence bandwidth, we define the bandwidth of $\mathcal{R}_{\mathrm{avg}}$ as the coherence bandwidth BW. There are different threshold values that may be chosen to define BW (e.g., half-power or e^{-1}). In this paper, we define the BW as the full width at half-maximum of the normalized $|\mathcal{R}_{\mathrm{avg}}|$ (normalized with respect to the peak value).

The rms delay spread τ_{rms} of the power delay profile $\mathrm{PDP}(t)$ for the chamber is discussed next. The $\mathrm{PDP}(t)$ in the chamber is given by [6]

$$\mathrm{PDP}(t) = \langle |h(t, n)|^2 \rangle \tag{5}$$

where the ensemble average is again taken over n, which represents the different samples. In this expression, $h(t, n)$ is the impulse response of the chamber for the nth sample, which is given by the inverse Fourier transform IFT of S_{21}:

$$h(t, n) = \mathrm{IFT}\left[S_{21_n}(f)\right]. \tag{6}$$

Once all values of S_{21_n} are measured and $\mathrm{PDP}(t)$ is found, τ_{rms} is obtained from the following [6]:

$$\tau_{\mathrm{rms}} = \sqrt{\frac{\int_0^\infty (t - \tau_0)^2 \mathrm{PDP}(t)\, dt}{\int_0^\infty \mathrm{PDP}(t)\, dt}} \tag{7}$$

where τ_0 is the mean delay of the propagation channel, given by

$$\tau_0 = \frac{\int_0^\infty t\, \mathrm{PDP}(t)\, dt}{\int_0^\infty \mathrm{PDP}(t)\, dt}. \tag{8}$$

Details for this calculation for different chamber environments are discussed in [6].

There is a connection between the Fourier transform FT of $\text{PDP}(t)$ and the function $\mathcal{R}_{\text{avg}}$ that is needed for determining the connection between τ_{rms} and BW. By use of the convolution theorem for time- and frequency-domain functions (or an inverted form of the Wiener–Khinchin–Einstein theorem or Wiener–Khintchine theorem [13]) it is shown that

$$\mathcal{R}_{\text{avg}} = \text{FT}\left[\text{PDP}(t)\right] = \langle \text{FT}[|h(t,n)|^2]\rangle$$
$$= \langle \text{FT}\left[h(t,n)\cdot h^*(t,n)\right]\rangle. \qquad (9)$$

Now, we discuss the last quantity used to characterize the chamber; that is, the chamber decay time τ_{RC}. The chamber decay time is often referred to as the chamber time constant. If we assume that the RC is a so-called well-performing chamber (which implies the chamber is well stirred with a large number of modes and a high mode density, see [1] and [14]), then the energy density, or the received power-delay spread in the chamber when the source is instantaneously turned OFF, is approximated by the following:

$$P(t) = \begin{cases} P_o\, e^{-t/\tau_{\text{RC}}} & t \geq 0 \\ 0 & t < 0 \end{cases} \qquad (10)$$

where τ_{RC} is the chamber decay time or chamber time constant. Through several years of experiments by various groups, it has been shown that this is a good approximation for late-time behavior of the RC. The chamber decay time is directly related to the losses in the chamber and, more importantly, related to the chamber Q by the following [1]:

$$\tau_{\text{RC}} = \frac{Q}{\omega}. \qquad (11)$$

It is logical to assume that τ_{RC} is related to BW and τ_{rms}. However, to obtain these relationships we need to make some assumptions about the early- and late-time behavior of the RC. What is typically done in the literature is to assume that the exponential behavior given in (10) is valid for all times in the chamber. That is, the ramp-up or charge-up time behavior of the chamber is neglected, and one assumes the power falls off exponentially starting at time zero. If we neglect the early-time behavior in the chamber, the $\text{PDP}(t)$ can be approximated by

$$\text{PDP}(t) = \langle |h(t,n)|^2\rangle = P_o e^{-t/\tau_{\text{RC}}}. \qquad (12)$$

Substituting this into (7) and (8), it can be shown that

$$\tau_o = \tau_{\text{rms}} = \tau_{\text{RC}}. \qquad (13)$$

If the expression in (12) is substituted into (9), it can be shown that [15]

$$|\mathcal{R}_{\text{avg}}|_{\text{norm}} = \frac{1}{\sqrt{1 + (2\pi f\, \tau_{\text{RC}})^2}} \qquad (14)$$

where the subscript refers to the normalized magnitude (normalized to its peak value). It is straightforward to show that the full-width bandwidth (that is, the coherence bandwidth) for the

TABLE I
COMPARISON OF BW_{meas} AND BW_{se} FOR VARIOUS LOADING CASES, WHERE $D\%$ IS THE PERCENT DIFFERENCE BETWEEN THESE TWO QUANTITIES

Chamber loading	τ_{rms} (ns)	BW_{meas} (MHz)	BW_{se} (MHz)	$D\%$ (%)
zero loading	1984.34	0.28	0.28	0.0
loading 1	566.41	0.97	0.98	1.0
loading 2	322.16	1.69	1.72	1.8
loading 3	224.77	2.40	2.46	2.5
loading 4	171.97	3.10	3.21	3.5
loading 5	125.62	4.18	4.39	5.0
loading 7	82.25	6.05	6.71	10.9

Since time gating was used to determine τ_{rms}, we have $\tau_{\text{rms}} = \tau_{\text{RC}}$.

half power of $|\mathcal{R}_{\text{avg}}|_{\text{norm}}$ is

$$\text{BW}_{\text{se}} = \frac{1}{\tau_{\text{RC}}}\frac{\sqrt{3}}{\pi} = \frac{1}{\tau_{\text{rms}}}\frac{\sqrt{3}}{\pi}$$

or

$$\tau_{\text{RC}} = \tau_{\text{rms}} = \frac{1}{\text{BW}_{\text{se}}}\frac{\sqrt{3}}{\pi} \qquad (15)$$

where the subscript "se" refers to the fact that a single-exponential model was used to derive this result. The expressions in (11) and (15) give the relationships between τ_{rms}, τ_{RC}, BW, and Q under the assumption that the time-domain behavior of the chamber is approximated by the single exponential function given in (12).

Experimental data for τ_{RC} and BW show the issues with the single-exponential model used to derive (15). Table I shows results for measured τ_{RC} and BW (referred to in this table as BW_{meas}) for various amounts of loading with radio-frequency (RF) absorber (referred to as chamber loading). In this table, we also show results for BW_{se}, where BW_{se} was obtained by substituting the measured τ_{RC} into the first of the expressions given in (15). The measurements were performed in one of the National Institute of Standards and Technology (NIST) RCs with dimensions of 2.9 m $\times$ 4.2 m $\times$ 3.6 m. The data presented in this table were obtained by performing S-parameter measurements with two horn antennas. The two antennas were pointed away from each other and pointed toward the two paddles in the chamber. In collecting these data, the stirrers (or paddles) were stepped to 100 different paddle positions. (Note that all the data presented later in this paper are for the same chamber and same antenna configuration.) The data presented in Table I correspond to a center frequency of 3.5 GHz, averaged over a 250-MHz bandwidth. For details on these types of measurement see [6]. The measured S-parameters were used in (3) to obtain $|\mathcal{R}_{\text{avg}}|$. From $|\mathcal{R}_{\text{avg}}|$, the half-power bandwidth was estimated to obtain BW (i.e., BW_{meas}). The values for τ_{rms} were obtained from (7), where the $h(t,n)$ needed to obtain $\text{PDP}(t)$ [see (5)] was found from the inverse Fourier transform of the measured S_{21}. Time-gating was used on the measured $\text{PDP}(t)$ in order to ensure that $\tau_{\text{RC}} = \tau_{\text{rms}}$ [as a consequence of the single

exponential assumption used to derive (15)]. In Section III-A, we discuss the time-gating approach used to determine τ_{rms}.

The results in Table I show a difference in $\mathrm{BW}_{\mathrm{meas}}$ and $\mathrm{BW}_{\mathrm{se}}$, with $\mathrm{BW}_{\mathrm{se}}$ overestimating the coherence bandwidth. The last column in this table shows the percent difference ($D\%$) between these two quantities. This difference illustrates that the expression given in (15) is, in general, not correct. The problem lies in the fact that the buildup time or early-time behavior of the chamber was neglected in determining these equations. We see that the difference is negligible for zero loading, but can become significant as the loading is increased. While for this chamber (and the loading used in it) we see differences of only up to 10%, much larger differences have been observed in other chambers with higher loading values. In fact, based on data presented in [16], the difference between the measured BW and $\mathrm{BW}_{\mathrm{se}}$ obtained by use of (15) is as high as 35% for high loading cases. In this paper, we discuss why this difference can be larger in some chambers, and discuss why the difference increases as the chamber loading is increased.

The assumption of the single-exponential model results in the presumed equality $\tau_{\mathrm{rms}} = \tau_{\mathrm{RC}}$. In general, because of the early-time behavior of the chamber, we have $\tau_{\mathrm{rms}} \neq \tau_{\mathrm{RC}}$. Others have observed this type of discrepancy [10] in RC measurements as well. While [10] gives a correction for relating τ_{rms} to τ_{RC} (where it is stated that $\tau_{\mathrm{rms}} = \sqrt{3}\,\tau_{\mathrm{RC}}$), this correction is constant and independent of chamber loading, and no physical explanation is given for this inequality. If one assumes the correction is constant for a given chamber, errors will result when the given chamber loading is changed. This type of error is illustrated in Fig. 2 of [17], where the assumption that $\tau_{\mathrm{rms}} = \sqrt{3}\tau_{\mathrm{RC}}$ (and the corresponding BW) results in an over-correction for an empty chamber and an under-correction for a heavily loaded chamber. Below we will give a physical explanation for this difference, where we explain that the problem is that the early-time behavior of the chamber's time-domain response is not taken into account. More importantly, we also show that the relative difference (or the ratio) in this early-time behavior to the chamber decay time τ_{RC} is a relevant parameter in assessing the validity of the single-exponential model, and hence any correction must be dependent on the chamber size and loading (since τ_{RC} is a function of chamber size and loading).

While loading an RC may seem counterintuitive, this is a common practice used in the testing of wireless devices in RCs [2], [6], [10], and [17]. In fact, certification and accreditation groups are in the process of developing international test methods that use this practice. While loading reduces the uniformity of the fields in the chamber [21], as one would expect, the chamber will still perform well as long as the chamber is not too heavily loaded. How much a chamber can be loaded is the topic of ongoing work from various groups [21]–[24].

The wireless community has investigated the relationship between BW and τ_{rms} for a number of years. It has been observed that in radio-propagation channels, the relationship between BW and τ_{rms} can be expressed as [11], and [18]–[20]

$$\mathrm{BW} = \frac{1}{k}\frac{1}{\tau_{\mathrm{rms}}} \tag{16}$$

TABLE II
DEFINITION OF PARAMETERS

Parameter	Definition
BW	coherence bandwidth
BW_{se}	coherence bandwidth derived from a single exponential model
BW_{de}	coherence bandwidth derived from a double exponential model
BW_{meas}	coherence bandwidth obtained from measurements
τ_{RC}	chamber decay time
τ_{rms}	RMS delay spread
τ_e	chamber early time (ramp-up or build-up time)
CR_{BW}	modification term for BW
$CR_{\tau_{RC}}$	modification term for τ_{RC}
$CR_{\tau_{rms}}$	modification term for τ_{rms}
k	radio-propagation environment constant

where k is a constant dependent on the radio-propagation environment. Values for k for different radio-propagation environments are given in [10], [11], and [18]–[20]. This k should not be confused with the Rician K factor that is often used to characterize a multipath propagation environment (including RC [2]). By use of (15) and (16), it can be shown that for a single-exponential model, $k = \pi/\sqrt{3}$. The deviation from $k = \pi/\sqrt{3}$ for other propagation environments is due to both the early- and late-time responses of those environments. Likewise, the fact that in general $k \neq \pi/\sqrt{3}$ for RC environments is due to the fact that the early-time behavior of the chamber is not correctly captured or described by a single-exponential model.

Various parameters are used in this paper. In order to facilitate the reading of this paper in the sections that follow, we have summarized the meaning of various parameters and terms in Table II.

III. DOUBLE EXPONENTIAL MODEL

The time behavior of NIST's chamber is shown in Fig. 1. This figure shows $\mathrm{PDP}(t)$ obtained from S_{21} data collected as discussed in the previous section. The S_{21} data used to obtain $\mathrm{PDP}(t)$ were collected over a frequency range of 1 to 6 GHz. This corresponds to a time resolution on the order of 0.17 ns, which is fine enough to resolve the initial wall reflections in the chamber. The data in this figure are indicative of data collected in other RCs, in that there is a time period (the early time) in which energy builds up in the chamber. After a given time, the $\mathrm{PDP}(t)$ for the different loading conditions approaches the late-time exponential behavior (i.e., $\ln[\mathrm{PDP}(t)]$ is linear versus t, as discussed in [1]); see Fig. 1(a) for $t > 100$ ns. Further observations indicate that the ramp-up (early-time) behavior is independent of the loading, see Fig. 1(b) for $t < 100$ ns. A double-exponential model would be a better representation of the chamber time-domain response as opposed to the single-exponential behavior given in (12). Thus, we assume that the time-domain chamber response is given by

$$\mathrm{PDP}(t) = \begin{cases} P_o\left[e^{-t/\tau_{\mathrm{RC}}} - e^{-t/\tau_e}\right] & t \geq 0 \\ 0 & t < 0 \end{cases} \tag{17}$$
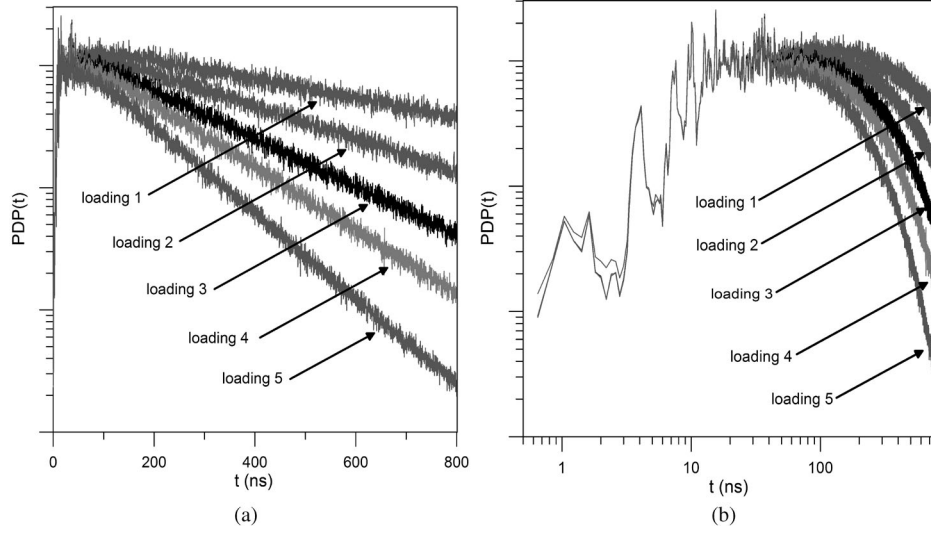
Fig. 1.   PDP(t) for different loading values: (a) linear scale to emphasize late-time behavior and (b) log scale to emphasize early-time behavior.

where τ_e is the chamber ramp-up time or early-time response and, as before τ_{RC}, is the late-time chamber decay time. The reason we chose the double exponential representation is twofold. We would like a functional form that captures the general behavior of the energy density (i.e., an increase from zero to a maximum value, then a decrease in an exponential manner). Second, we would like a functional form that allows us to analytically calculate the relationships between the four chamber characterization quantities in order to illustrate the effects of the early-time response. The double-exponential functional form meets these criteria. Obviously the double-exponential model cannot capture the exact early-time behavior of each individual ray in chamber. The intent of the double-exponential model is to have an expression that can capture the general or "average" tendency of the early-time energy buildup in the chamber.

Fig. 2 illustrates examples of the functional form of the double-exponential model for different $\tau_{\mathrm{RC}}/\tau_e$. This figure shows how the early-time behavior changes as a function of $\tau_{\mathrm{RC}}/\tau_e$. In Section III-B, we show how well this model represents actual measured PDP(t) for different chamber loadings.

Substituting (17) into (9) we have

$$\mathcal{R}_{\mathrm{avg}} = P_o \left[\frac{\tau_{\mathrm{RC}}}{1 + 2j\pi f\, \tau_{\mathrm{RC}}} - \frac{\tau_e}{1 + 2j\pi f\, \tau_e} \right]. \tag{18}$$

The magnitude of this function normalized to the peak is given by

$$|\mathcal{R}_{\mathrm{avg}}|_{\mathrm{norm}} = \frac{1}{\sqrt{[1 - (2\pi f)^2 \tau_{\mathrm{RC}}\, \tau_e]^2 + (2\pi f)^2 (\tau_{\mathrm{RC}} + \tau_e)^2}}. \tag{19}$$

Setting this normalized function to 0.5, the following relationship is obtained for BW and τ_{RC}:

$$\mathrm{BW}_{\mathrm{de}} = \frac{1}{\tau_{\mathrm{RC}}} \frac{\sqrt{3}}{\pi} CR_{\mathrm{BW}} \tag{20}$$
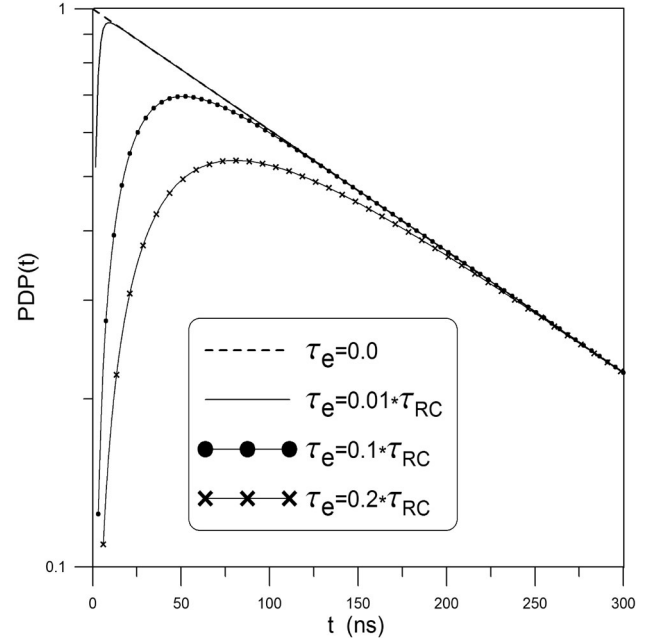
Fig. 2.   Illustration of the double-exponential model for PDP(t) for various values of $\tau_{\mathrm{RC}}/\tau_e$, with $\tau_{\mathrm{RC}} = 200$ ns.

where the subscript "de" corresponds to the double-exponential model and

$$\tau_{\mathrm{RC}} = \frac{1}{\mathrm{BW}_{\mathrm{de}}} \frac{\sqrt{3}}{\pi} CR_{\tau_{\mathrm{RC}}} \tag{21}$$

where CR_{BW} and $CR_{\tau_{\mathrm{RC}}}$ are modification terms that account for the early-time response of the chamber and are given by

$$CR_{\mathrm{BW}}$$
$$= \frac{1}{\sqrt{6}} \sqrt{\left[\left(\frac{\tau_{\mathrm{RC}}}{\tau_e} \right)^4 + 14 \left(\frac{\tau_{\mathrm{RC}}}{\tau_e} \right)^2 + 1 \right]^{1/2} - \left(\frac{\tau_{\mathrm{RC}}}{\tau_e} \right)^2 - 1} \tag{22}$$
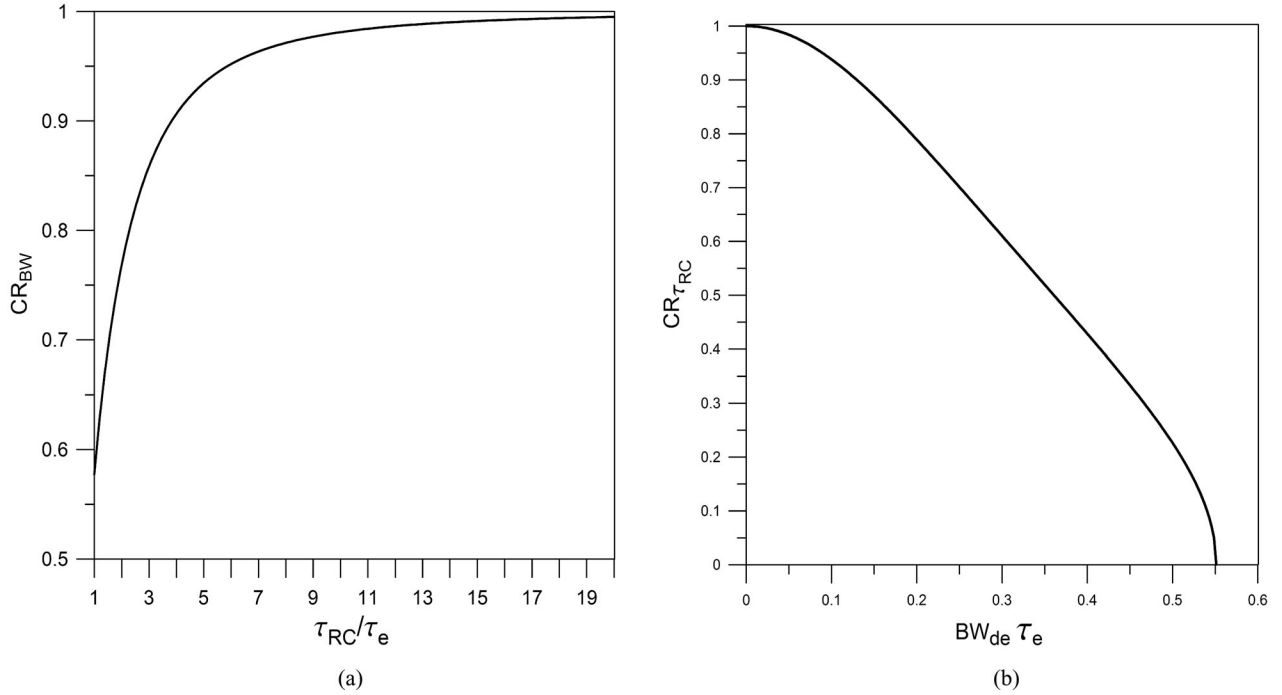
Fig. 3.   Modification terms for the double-exponential model for PDP(t): (a) CR_{BW}, and (b) $CR_{\tau_{\mathrm{RC}}}$.

and

$$CR_{\tau_{\mathrm{RC}}} = \sqrt{\frac{1 - \frac{\pi^2}{3} \left(\mathrm{BW}_{\mathrm{de}}\tau_e\right)^2}{1 + \pi^2 \left(\mathrm{BW}_{\mathrm{de}}\tau_e\right)^2}}. \tag{23}$$

We see that under the double-exponential approximation, the relationship between τ_{RC} and BW is more complicated than that given in (15). Fig. 3(a) shows the functional form of (22). It can be shown that the limit as $\tau_{\mathrm{RC}}/\tau_e$ approaches ∞ results in $CR_{\mathrm{BW}} \to 1$, and hence, the expression in (20) reduces to that given in (15). The expression for CR_{BW} is valid only for $\tau_{\mathrm{RC}} \geq \tau_e$ (recall that when $\tau_{\mathrm{RC}} = \tau_e$, PDP$(t) = 0$). From (23), if $\mathrm{BW}_{\mathrm{de}}\tau_e$ is "very small" then the modification is small, and, as $\mathrm{BW}_{\mathrm{de}}\tau_e \to 0$, $CR_{\tau_{\mathrm{RC}}} \to 1$ [(21) reduces to that given in (15)]. The expression for $CR_{\tau_{\mathrm{RC}}}$ is valid only for $\mathrm{BW}_{\mathrm{de}}\tau_e \geq \sqrt{3}/\pi$, where, from (17), this corresponds to the time where $\tau_{\mathrm{RC}} = \tau_e$. Fig. 3(b) shows the functional form of this expression.

Next, we derive τ_{rms} for the double-exponential function. This is done by substituting (17) into (7). Thus,

Fig. 4. $CR_{\tau_{\mathrm{rms}}}$ for the double-exponential model for PDP(t) for various $\tau_e/\tau_{\mathrm{RC}}$.

by

$$\tau_{\mathrm{rms}} = \tau_{\mathrm{RC}} \, CR_{\tau_{\mathrm{rms}}} \quad \text{and} \quad CR_{\tau_{\mathrm{rms}}} = \sqrt{1 + \left(\frac{\tau_e}{\tau_{\mathrm{RC}}}\right)^2}. \tag{24}$$

As before, this expression is valid only for $\tau_{\mathrm{RC}} \geq \tau_e$. Under this condition, the term has a maximum value of $\sqrt{2}$. Fig. 4 shows the functional form of this expression.

Finally, using the definition in (16), it can be shown that the expression for k for the double-exponential model is given
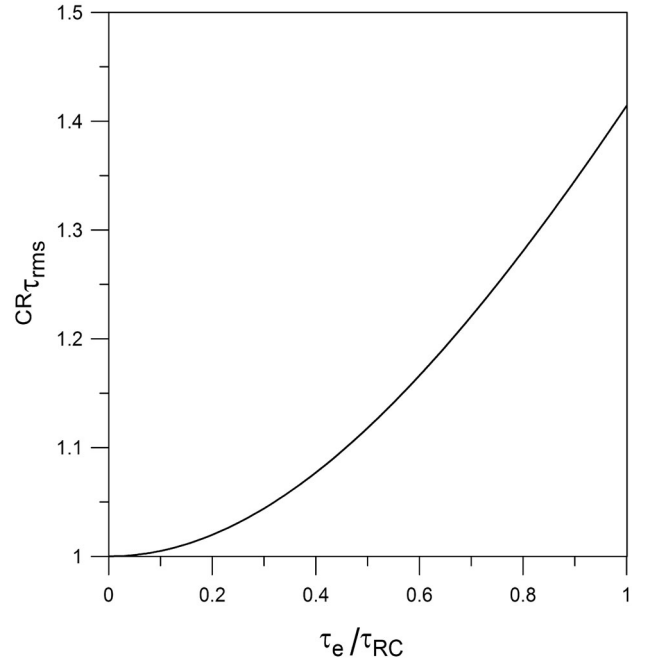
$$k = \frac{\pi}{\sqrt{3}} \sqrt{\frac{6\left(1 - \left(\frac{\tau_e}{\tau_{\mathrm{rms}}}\right)^2\right)}{\left[\left(\frac{\tau_{\mathrm{rms}}}{\tau_e}\right)^4 + 12\left(\frac{\tau_{\mathrm{rms}}}{\tau_e}\right)^2 - 12\right]^{1/2} - \left(\frac{\tau_{\mathrm{rms}}}{\tau_e}\right)^2}}. \tag{25}$$
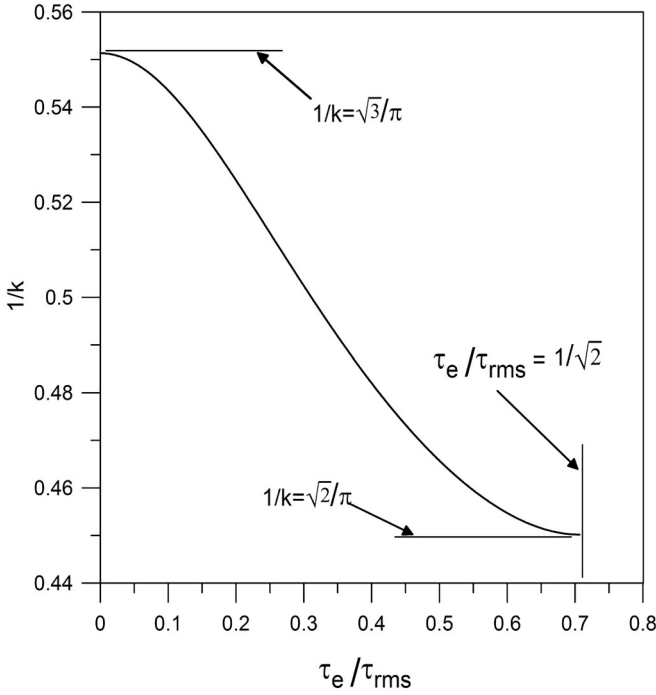
Fig. 5. k for the double-exponential model for PDP(t) for various $\tau_e/\tau_{\rm rms}$.

Fig. 5 shows a plot of $1/k$ versus $\tau_e/\tau_{\rm rms}$. The factor $1/k$ has a maximum value of $\sqrt{3}/\pi$ (at $\tau_e = 0$) and a minimum of $\sqrt{2}/\pi$ (at $\tau_e/\tau_{\rm rms} = 1/\sqrt{2}$, which corresponds to $\tau_e = \tau_{\rm RC}$).

A. Relating $\tau_{\rm rms}$ to $\tau_{\rm RC}$

A few comments are needed regarding when the conditions $\tau_{\rm rms} = \tau_{\rm RC}$ is an accurate approximation, and how one can determine $\tau_{\rm RC}$ from experimental data. In general, $\tau_{\rm rms} \neq \tau_{\rm RC}$, and as mentioned earlier, we see that $\tau_{\rm RC} \approx \tau_{\rm rms}$ only when $\tau_e/\tau_{\rm RC} \ll 1$. Thus, a measurement of $\tau_{\rm rms}$ is not a direct measurement of $\tau_{\rm RC}$. Besides using the expression given in (24), how does one obtain $\tau_{\rm RC}$?

From (11), we know $\tau_{\rm RC} = Q/\omega$. The Q in this expression should only have contributions from losses associated with the chamber and not losses associated with the antennas used in the measurement. One approach to measure Q is from (2), where a measurement of S_{21} is obtained from two antennas placed in a chamber. However, as discussed in [7]–[9], such a measurement of Q has losses associated with both the chamber and losses associated with the nonideal antennas. With the idea that we are interested in the Q associated with only the chamber losses, the antenna losses would have the effect of reducing Q from that of the Q for ideal antennas, and hence Q measured in this manner [i.e., the use of (2)] would underestimate $\tau_{\rm RC}$ when (11) is used. Thus, unless one knows the antenna efficiencies and corrects for them (see [8] and [9]), this approach will give erroneous results, and a different approach is needed.

An alternative approach for determining $\tau_{\rm RC}$ is based on time gating the measured PDP(t). The technique is as follows. The PDP(t) from measured S_{21} is first determined from (5). One then determines the delay (i.e., the time) in the PDP(t) when the chamber has reached a point where the response of the chamber is clearly decaying exponentially. Once this delay t_d is determined, the PDP(t) is then time-gated by simply shifting the time zero point of the PDP(t) to t_d. $\tau_{\rm rms}$ is then calculated from (7) with the time-gated PDP(t). If the chamber response is truly exponential for its late-time response and one can correctly gate the early-time behavior of PDP(t), then $\tau_{\rm RC}$ is this time-gated value of $\tau_{\rm rms}$.

The aforementioned approach for determining $\tau_{\rm RC}$ works, provided that the time delay for the time-gating process is chosen correctly. There are a few techniques that can be used to determine t_d. One approach is to choose a t_d and use (7) and (8) to determine $\tau_{\rm rms}$ and τ_o. If the time-gated PDP(t) is truly exponential, $\tau_{\rm rms} = \tau_o$ and both will equal $\tau_{\rm RC}$. t_d is sequentially increased until the calculated $\tau_{\rm rms} - \tau_o \leq \epsilon$, where ϵ is an acceptably small value. At this point, $\tau_{\rm rms} \simeq \tau_{\rm RC}$. One can add an additional criterion, if desired, by noting that if the chamber is truly exponential, then for late times the slope of $\ln[\text{PDP}(t)]$ will be equal to $1/\tau_{\rm RC}$ (or $1/\tau_{\rm rms}$), if t_d is chosen large enough. The slope can be added to the aforementioned conditions for determining $\tau_{\rm RC}$.

Another approach for determining t_d is based on the work done in acoustic RC. Various researchers have defined a mean-free-path length as [25]–[29]

$$l_c = \frac{4V}{S_A} \qquad (26)$$

where V and S_A are the volume and surface area of the chamber, respectively. Using the mean-free-path length, a characteristic room time is defined in [4], as

$$t_c = \frac{2l_c}{c} = \frac{8V}{cS_A} \qquad (27)$$

where c is the speed of light in vacuum. Note that some authors in acoustics define a characteristic room time as $\frac{4V}{cS_A}$. This time [as expressed in (27)] is defined as the time required before a given set of rays makes one reflection in a room (or chamber), see [4] for details. Dunens and Lambert [3] have shown that after $4t_c$ the energy in acoustic chambers has built up to a fully reverberant stage, [4] states that this reverberation condition occurs after $5t_c$, and [5] concludes that the reverberation condition occurs between $4t_c$ to $5t_c$. Thus, an approximation for the delay needed for time-gating is $t_d \approx 5t_c$. There is more discussion on t_d below (where experimental data are used to justify the conclusion that the reverberant behavior occurs by $5t_c$), as well as a discussion on the use of this characteristic chamber (or room) time t_c to approximate the early-time constant τ_e.

B. Discussion On τ_e and $\tau_e/\tau_{\rm RC}$

For a given chamber size, the modification terms $CR_{\rm BW}$, $CR_{\tau\rm RC}$, and $CR_{\tau\rm rms}$ are not constant for different loading configurations, and depend on the ratio $\tau_e/\tau_{\rm RC}$ (which is a comparison of the early-time to the late-time behavior of the chamber). In general, this ratio will be different for every RC and every loading configuration. As we discussed earlier, τ_e and $\tau_{\rm RC}$ are characteristics of the particular chamber being used. The time constant $\tau_{\rm RC}$ is a function of both the chamber size

and losses in the chamber, as shown in (11), and in Fig. 1(a). The time constant τ_{RC} can change significantly with loading, which is discussed in [6]. On the other hand, the early-time time behavior of the chamber is dominated by the chamber size, and for the most part, is independent of the chamber loading [see Fig. 1(b)]. The assumption that τ_e is a function of the chamber size is discussed in [3]. Therefore, as one changes the loading in the chamber, the modification terms will change, due to the change in τ_{RC}, rather than a change in τ_e.

The time constant τ_e can be approximated in various ways. One approach is to determine BW and τ_{RC} from measured data. The BW of $\langle \mathcal{R}(f) \rangle$ can be obtained from measured values of the chamber's S-parameters, and τ_{RC} can be obtained from (7) once the early-time behavior of the chamber is time-gated from the PDP(t). Once we have experimentally obtained $\mathrm{BW}_{\mathrm{meas}}$ and τ_{RC}, (21) and (23) are used to obtain τ_e with the following:

$$\tau_e = \frac{1}{\mathrm{BW}_{\mathrm{meas}}} \frac{\sqrt{3}}{\pi} \sqrt{\frac{1 - \frac{\pi^2}{3} \left(\mathrm{BW}_{\mathrm{meas}} \tau_{\mathrm{RC}} \right)^2}{1 + \pi^2 \left(\mathrm{BW}_{\mathrm{meas}} \tau_{\mathrm{RC}} \right)^2}}. \tag{28}$$

A second approach is based on curve fitting the measured PDP(t) to the double-exponential model in order to determine τ_{RC} and τ_e. There are different methods for fitting the measured PDP(t). One approach is to first determine τ_{RC} from the time-gating method discussed earlier. This τ_{RC} is used in the double-exponential model given in (17), and τ_e in this double-exponential model is then obtained by curve-fitting (17) to the measured PDP(t). Fig. 6 illustrates the measured PDP(t) (obtained from the inverse Fourier Transform of the measured S_{21}) for various chamber loading values. In these curves, we have also plotted the double-exponential model. τ_{RC} for each of the different loadings was obtained from the time-gating approach, and τ_e then determined from fitting (17) to the various datasets. The values of τ_{RC} and τ_e are shown in the plots. From these plots, we see that the double-exponential model represents the early-time and late-time PDP(t) of the chamber.

As we stated earlier, the early-time behavior is independent of the chamber loading and thus, for a given chamber, τ_e should be constant for different loadings. The curve-fitting approach for the different chamber loadings gave a chamber early-time time constant of approximately 22 ns (averaging the different values given in Fig. 6). Since τ_e is independent of chamber loading and is a function of only the chamber geometry, one can obtain an approximate expression for τ_e. The early-time behavior of the chamber is dominated by the time it takes the first set of rays leaving a transmitting antenna and arriving at the receiving antenna after making one reflection off of the walls and paddles. After this initial ramp-up time, rays making multiple bounces continually arrive until reverberant behavior is developed in the chamber (after $t > 5t_c$). As discussed earlier, the characteristic room (or chamber) time, as defined in [4], accounts for the initial ramp-up time associated with rays making one bounce off the reflecting surfaces. Thus, the characteristic room time t_c can be used to approximate the early-time time constant:

$$\tau_e \approx t_c = \frac{8V}{cS_A}. \tag{29}$$

TABLE III
COMPARISON OF τ_e OBTAINED FROM THE THREE APPROACHES
FOR VARIOUS LOADINGS

Chamber loadings	τ_{RC} (ns)	τ_e (ns) Eq. 28	τ_e (ns) curve fitted	$\tau_e \approx t_c$ (ns) Eq. 29	$\tau_e \approx \frac{3}{2}t_c$ (ns) Eq. 30
loading 0	1984.34	–	20.0	15.4	23.1
loading 2	322.16	19.5	23.0	15.4	23.1
loading 3	224.77	22.5	24.5	15.4	23.1
loading 4	171.97	22.6	22.1	15.4	23.1
loading 5	125.62	21.1	23.1	15.4	23.1
loading 7	82.25	21.2	20.2	15.4	23.1

By use of the dimensions for the chamber in this dataset (2.9 m × 4.2 m × 3.6 m), the duration of the early-time behavior is $\tau_e \approx 15.4$ ns. This value for τ_e is used in the double-exponential model and is also plotted in Fig. 6. This figure compares the measured PDP(t) with the double-exponential model for τ_e obtained from curve fitting and from the approximate expression. The results in this figure illustrate that the double-exponential model with the approximate expression for τ_e (for $\tau_e = 15.4$ ns) may be used to represent both the early-time and late-time behavior of the measured PDP(t). In these plots, we have also indicated t_c and $5t_c$. We see that $5t_c = 77$ ns does correspond to where the measured PDP(t) develops into the reverberant behavior and is represented by a single-exponential model.

Table III compares τ_e, obtained from all three techniques, i.e., from (28), from curve fitting, and from (29) (where $\tau_e = t_c$). We see that the curve fitting and the results from (28) give similar results, while the results obtained from $\tau_e = t_c$ underestimate τ_e when compared to the other two approaches. When comparing the results in Table III, we see that a better approximation for τ_e may be

$$\tau_e \approx \frac{3}{2}t_c = \frac{12V}{cS_A}. \tag{30}$$

Values for this approximation are also shown in Table III, which correspond better than the results obtained from curve fitting than to those obtained from (29). To further illustrate that some multiplier of t_c captures the ramp-up time of a chamber, we used (29) and (30) for the dimensions of a square chamber given in [30], which gives $t_c = 7.8$ ns and $3t_c/2 = 12$ ns, respectively. When compared to the time-domain data discussed [30], we see that 7 to 12 ns corresponds to the early-time behavior (or the time for the first set of rays to arrive at a test point) of the square chamber. We see that the approximation given in (30) corresponds better to curves given in [30]. Future work will include investigating how well this expression represents the early-time behavior of other chambers.

C. Comparison of BW_{se} and BW_{de} to Measurements

In this section, we investigate the validity of BW obtained from the double-exponential model [or (20)]. Table IV shows a comparison for measured BW (obtained from $\langle \mathcal{R}(f) \rangle$, and referred to as $\mathrm{BW}_{\mathrm{meas}}$) to BW obtained from (20) for different loadings. The values for τ_{rms} in the table are the same as those
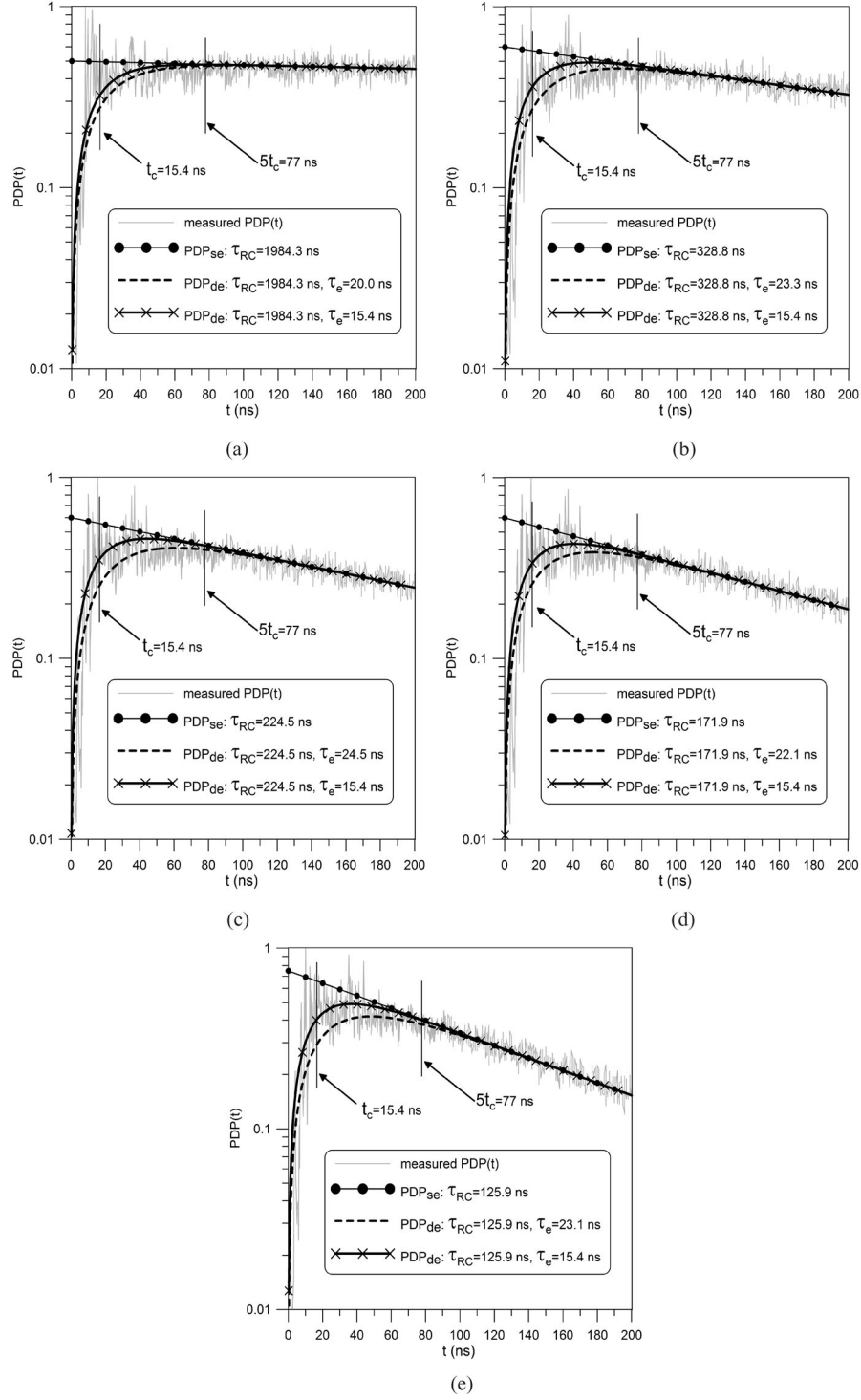
Fig. 6.　Comparison of the double-exponential model to measured $PDP(t)$, (a) zero-absorber, (b) loading 2 (two pieces of absorber), (c) loading 3 (three pieces of absorber), (d) loading 4 (four pieces of absorber), and (e) loading 5 (five pieces of absorber).

used in Table I and were obtained from (7), where the values of $h(t, n)$ needed to obtain $PDP(t)$ in (5) were obtained from the inverse Fourier transform of the measured S_{21}. Time-gating was used on $PDP(t)$ in order to ensure that $\tau_{\mathrm{rms}} = \tau_{\mathrm{RC}}$. In the table, we show the calculated BW_{de} [from (20)] for τ_e obtained from both the curve fitting value given in Fig. 6, and from τ_e obtained from (29) and (30) [i.e., $\tau_e = \tau_c = 15.4$ ns and

$\tau_e = 3\tau_c/2 = 23.1$ ns]. We show the percent difference ($D\%$) between BW_{meas} and BW_{de} for the different values for τ_e; we also show BW_{se} and its corresponding $D\%$.

The first thing we notice is that the modification for BW (relative to BW_{se}) as given in (20) is smaller for small amounts of chamber loading and larger for larger chamber loading. As stated before, this is due to the fact that early-time behavior is

TABLE IV
COMPARISON OF BW_{meas} AND BW_{de} FOR VARIOUS LOADING CONDITIONS

Chamber loading	$\tau_{rms} = \tau_{RC}$ (ns)	BW_{meas} (MHz)	BW_{se} (MHz)	BW_{de} (MHz)		
zero loading	1984.3	0.276	$BW_{se} = 0.28$ $D\% = 0.0$	$\tau_e = 20.0$ ns $BW_{de} = .278$ $D\% = 0.7$ $\tau_{RC}/\tau_e = 99.2$	$\tau_e = 15.4$ ns $BW_{de} = .278$ $D\% = 0.7$ $\tau_{RC}/\tau_e = 128.9$	$\tau_e = 23.1$ ns $BW_{de} = .278$ $D\% = 0.7$ $\tau_{RC}/\tau_e = 85.9$
loading 2	322.16	1.699	$BW_{se} = 1.72$ $D\% = 1.8$	$\tau_e = 23.3$ ns $BW_{de} = 1.694$ $D\% = 0.03$ $\tau_{RC}/\tau_e = 13.8$	$\tau_e = 15.4$ ns $BW_{de} = 1.703$ $D\% = 0.2$ $\tau_{RC}/\tau_e = 20.9$	$\tau_e = 23.1$ ns $BW_{de} = 1.694$ $D\% = 0.03$ $\tau_{RC}/\tau_e = 13.9$
loading 3	224.77	2.40	$BW_{se} = 2.46$ $D\% = 2.5$	$\tau_e = 24.5$ ns $BW_{de} = 2.40$ $D\% = 0.8$ $\tau_{RC}/\tau_e = 9.2$	$\tau_e = 15.4$ ns $BW_{de} = 2.43$ $D\% = 0.8$ $\tau_{RC}/\tau_e = 14.6$	$\tau_e = 23.1$ ns $BW_{de} = 2.404$ $D\% = 0.2$ $\tau_{RC}/\tau_e = 9.7$
loading 4	171.97	3.105	$BW_{se} = 3.21$ $D\% = 3.5$	$\tau_e = 22.1$ ns $BW_{de} = 3.1105$ $D\% = 0.2$ $\tau_{RC}/\tau_e = 7.8$	$\tau_e = 15.4$ ns $BW_{de} = 3.15$ $D\% = 1.4$ $\tau_{RC}/\tau_e = 11.2$	$\tau_e = 23.1$ ns $BW_{de} = 3.101$ $D\% = 0.13$ $\tau_{RC}/\tau_e = 7.4$
loading 5	125.62	4.177	$BW_{se} = 4.39$ $D\% = 5.0$	$\tau_e = 23.1$ ns $BW_{de} = 4.131$ $D\% = 1.1$ $\tau_{RC}/\tau_e = 5.4$	$\tau_e = 15.4$ ns $BW_{de} = 4.25$ $D\% = 1.7$ $\tau_{RC}/\tau_e = 8.2$	$\tau_e = 23.1$ ns $BW_{de} = 4.139$ $D\% = 0.91$ $\tau_{RC}/\tau_e = 5.4$
loading 7	82.25	6.05	$BW_{se} = 6.71$ $D\% = 10.9$	$\tau_e = 20.2$ ns $BW_{de} = 6.09$ $D\% = 0.7$ $\tau_{RC}/\tau_e = 4.1$	$\tau_e = 15.4$ ns $BW_{de} = 6.31$ $D\% = 4.3$ $\tau_{RC}/\tau_e = 5.3$	$\tau_e = 23.1$ ns $BW_{de} = 5.958$ $D\% = 1.45$ $\tau_{RC}/\tau_e = 3.6$

Because time-gating was used to determine τ_{rms}, we have $\tau_{rms} = \tau_{RC}$.

less important for chambers with large chamber time-constants relative to τ_e. From these comparisons, we see that the single exponential model for BW_{se} overestimates BW, while the double exponential model better corresponds to the measured BW. We also see the BW_{de} values obtained from $\tau_e = \tau_c$ give larger values for BW (or over estimates BW) compared to those obtained using τ_e from the curve fitting, where the amount of the underestimation is larger for larger chamber loading. This illustrates that t_c may underestimate τ_e. In this table, we show values of BW_{de} obtained from $\tau_e = 3\tau_c/2 = 23.1$ ns, which more closely follow those obtained when τ_e is obtained from curve fitting. Improving the approximation for t_c is the topic of further work.

As discussed earlier, the ratio τ_{RC}/τ_e can be used as means to distinguish when the early-time behavior in the chamber is important in determining BW for different chamber loading conditions. This ratio is also shown in Table IV. As one would expect, this ratio decreases with loading (since τ_{RC} decreases with loading), indicating that the early-time behavior is important and quantities derived from a simple single-exponential model may be in question.

In order to further illustrate that the early-time behavior of the chamber causes the narrowing of the actual measured coherence BW when compared to the BW_{se}, we have performed

TABLE V
COMPARISON OF BW_{meas} AND BW_{de} FOR VARIOUS LOADING CONDITIONS

Chamber loading	BW_{meas} (MHz)	$BW_{meas,TG}$ (MHz)	BW_{se} (MHz)
zero loading	0.276	.277	0.276
loading 1	0.972	0.978	0.980
loading 2	1.699	1.72	1.737
loading 3	2.403	2.49	2.496
loading 4	3.105	3.25	3.251
loading 5	4.177	4.41	4.491
loading 7	6.048	6.56	6.70

Because time-gating was used to determine τ_{rms}, we have $\tau_{rms} = \tau_{RC}$.

the following analysis: we first take the $PDP(t)$ obtained from measured S_{21}, and time-gate the $PDP(t)$ to a point where the $PDP(t)$ in the chamber has reached reverberant behavior. This time-gated $PDP(t)$ is then Fourier-transformed back to the frequency domain. The coherence bandwidth is then obtained from the time-gated frequency-domain data. Table V shows a comparison of the time-gated BW_{meas}, TG (where the subscript refers to time-gated measured data), to BW_{se} obtained from (15). Also

shown in the table is the $\mathrm{BW_{meas}}$ obtained for nontime-gated data. The data in this table show that once the data are time-gated to remove the early-time chamber behavior, the coherence bandwidth of the time-gated data correspond very well to those obtained from (15). This illustrates that the early-time behavior is why the coherence bandwidth of nontime-gated data for $\langle \mathcal{R}(f) \rangle$ cannot in general be obtained from the single-exponential model [or (15)].

A detailed discussion of the uncertainties associated with these types of RC measurements is given in [8]. In [8], the uncertainties associated with instrumentation drift, paddle averaging, frequency averaging, and position averaging are discussed.

IV. CONCLUSION AND DISCUSSION

We presented a double-exponential model that accounts for the early-time behavior of the chamber that can be used to develop relationships between BW, τ_{RC}, and/or τ_{rms}. We also presented expressions relating these quantities. This model helps one understand how the early-time behavior of the chamber can affect the relationships between the various quantities (τ_{rc}, τ_{rms}, BW, and k) for both loaded and unloaded chambers.

The double-exponential model for the chamber presented here requires knowledge of the chamber decay time τ_{RC} and the ramp-up time of the chamber τ_e. We discussed how one determines τ_{RC} from the τ_{rms}, in which τ_{rms} is obtained from measured data. We also discussed three approaches for determining τ_e. One approach is based on the relationship between BW and τ_e, a second is based on curve-fitting, and a third is based on two approximate expressions. The equations for τ_e (in terms of the characteristic room time, t_c) are expressed in terms of only the chamber volume and surface area, and hence are independent of the chamber loading (as would be expected). Further work will include investigating chambers of different sizes and loadings in order to understand the validity of these approximate expressions for τ_e. We also illustrated that the ratio $\tau_{\mathrm{RC}}/\tau_e$ can be used as means to distinguish when the early-time behavior in the chamber is important for different chamber loading conditions. This ratio decreases with loading, indicating that the early-time behavior is important and quantities derived from a simple single-exponential model may be in question.

While the double-exponential model may not exactly represent early-time behavior, it does illustrate the problem with not accounting for the early-time behavior of the chamber. In fact, this early time behavior has the effect of reducing (or narrowing) the RC's coherence bandwidth over that obtained when one assumes a single-exponential behavior for the chamber. This double exponential represents the global behavior of the chamber and allows one to derive relationships between BW, τ_{RC}, and τ_{rms} in the chamber. The relationships between these quantities allow one to interpret and interchange experimental data of $\mathrm{PDP}(t)$ and $\langle \mathcal{R}(f) \rangle$. In future work, we will look at different chamber sizes in order to further investigate the validity of the double-exponential model, and look at other types of functional forms that could be used as models for predicting the early-time behavior of the RC.

REFERENCES

[1] D. A. Hill, *Electromagnetic Fields in Cavities: Deterministic and Statistical Theories.* New York: IEEE Press, 2009.
[2] C. L. Holloway, D. A. Hill, J. M. Ladbury, P. F. Wilson, G. Koepke, and J. Code, "On the use of reverberation chambers to simulate a controllable Rician radio environment for the testing of wireless devices," *IEEE Trans. Antennas Propag., Special Issue Wireless Commun.*, vol. 54, no. 11, pp. 3167–3177, Nov. 2006.
[3] E. K. Dunens and R. F. Lambert, "Impulsive sound-level response statistics in a reverberant enclosure," *J. Acoust. Soc. Amer.*, vol. 61, no. 6, pp. 1524–1532, 1977.
[4] C. L. Holloway, M. G. Cotton, and P. McKenna, "A model for predicting the power delay profile characteristics inside a room," *IEEE Trans. Veh. Technol.*, vol. 48, no. 4, pp. 1110–1120, Jul. 1999.
[5] R. E. Richardson, "Reverberant microwave propagation," Naval Surface Warfare Center, Dahlgren, VA, Tech. Rep. NSWCDD/TR-08/127, Oct. 2008.
[6] E. Genender, C. L. Holloway, K. A. Remley, J. M. Ladbury, and G. Koepke, "Simulating the multipath channel with a reverberation chamber: Application to bit error rate measurements," *IEEE Trans. Electromagn. Compat.*, vol. 52, no. 4, pp. 766–777, Nov. 2010.
[7] H. G. Krauthauser and M. Herbrid, "Yet another antenna efficiency measurement method in reverberation chambers," in *Proc. IEEE Int. Symp. Electromagn. Compat.*, Fort Lauderdale, FL, Jul. 25–20, 2010, pp. 536–540.
[8] C. L. Holloway, H. Shah, R. J. Pirkl, W. Young, J. Ladbury, and D. A. Hill, "Reverberation chamber techniques for determining the radiation and total efficiency of antennas," *IEEE Trans. Antennas Propag.*, accept for publication in Apr. 2012 and is available at IEEE Xplore early access.
[9] C. L. Holloway, H. A. Shah, R. J. Pirkl, D. A. Hill, and J. Ladbury, "A three-antenna technique for determining the efficiency of antennas," presented at the 2011 33rd Symp. Antenna Meas. Tech. Assoc., Denver, CO, Oct. 16–21, Oct. 2011.
[10] X. Chen, P.-S. Kildal, C. Orlenius, and J. Carlsson, "Channel sounding of loaded reverberation chambers for over-the-air testing of wireless devices-coherence bandwidth versus average mode bandwidth and delay spread," *IEEE Antennas Wireless Propag. Lett.*, vol. 8, pp. 678–681, 2009.
[11] W. C. Jakes, *Microwave Mobile Communications.* New York: IEEE Press, 1993.
[12] J. G. Proakis, *Digital Communications*, 2nd ed. New York: McGraw-Hill, 1989, ch. 7.
[13] R. N. Bracewell, *The Fourier Transform and Its Applications.* New York: McGraw-Hill, 1999.
[14] R. E. Richardson, "Mode-stirred calibration factor, relaxation time, and scaling laws," *IEEE Trans. Instrum. Meas.*, vol. 34, no. 4, pp. 573–580, Dec. 1985.
[15] E. O. Brighamn, *The Fast Fourier Transform and its Applications.* Englewood Cliffs, NJ: Prentice-Hall, 1988.
[16] X. Chen and P.-S. Kildal, "Relations between coherence bandwidth and average mode bandwidth in reverberation chamber for wireless device measurements," in *Proc. 2008 Int. Symp. Antenna Propag.*, Taipei, Taiwan, Oct. 2008, pp. 27–30.
[17] X. Chen and P.-S. Kildal, "Comparison of RMS delay spread and decay time measured in reverberation chamber," presented at the 4th Eur. Conf. Antennas Propag., Barcelona, Apr. 12–16, 2010.
[18] T. S. Rappaport, *Wireless Communications: Principles and Practice.* Upper Saddle River, NJ: Prentice-Hall, 1996.
[19] G. J. M. Janssen, P. A. Stigter, and R. Prasad, "Wideband indoor channel measurements and BER analysis of frequency selective multipath channels at 2.4, 4.75, and 11.5 GHz," *IEEE Trans. Commun.*, vol. 44, no. 10, pp. 127–212, Oct. 1996.
[20] B. H. Fleury, "An uncertainty relation for WSS processes and its application to WSSUS systems," *IEEE Trans. Commun.*, vol. 44, no. 12, pp. 1632–1634, Dec. 1996.
[21] C. L. Holloway, D. A. Hill, J. M. Ladbury, and G. Koepke, "Requirements for an effective reverberation chamber: Unloaded or loaded," *IEEE Trans. Electromagn. Compat.*, vol. 48, no. 1, pp. 187–194, Feb. 2006.
[22] B. Zhang, W. Li, X. Li, Z. Yuan, J. He, and R. Zeng, "Load effect investigation of a reverberation chamber," in *Proc. 8th Int. Symp. Antennas, Propag. EM Theory*, Nov. 2–5, 2008, pp. 1115–1118.
[23] O. Lunden and M. Backstrom, "Absorber loading study in FOI 36.7 m3 mode stirred reverberation chamber for pulsed power measurements," in *Proc. IEEE Int. Symp. Electromagn. Compat.*, Detroit, MI, Aug. 18–22, 2008, pp. 1–5.

[24] *EMC, Part 4: Testing and measurement techniques; Section 21: Reverberation chamber test methods, International Electrotechnical Commission,* Committee Draft, Geneva, IEC 61000-4-21, 2001.

[25] A. D. Pierce, *Acoustics: An Introduction to Its Physical Principles and Applications.* New York: McGraw-Hill, 1981, ch. 6.

[26] C. W. Kosten, "The mean free path in room acoustics," *Acoustica*, vol. 10, pp. 245–250, 1960.

[27] F. V. Hunt, "Remarks on the mean free path problem," *J. Acoust. Soc. Amer.*, vol. 36, no. 3, pp. 556–564, 1964.

[28] L. Batchelder, "Reciprocal of the mean free path," *J. Acoust. Soc. Amer.*, vol. 36, no. 3, pp. 551–555, 1964.

[29] H. Kuttruff, *Room Acoustics..* Norfolk, U.K.: Applied Science, 1973, ch. 5.

[30] D.-H. Kwon, R. J. Burkholder, and P. H. Pathak, "Ray analysis of electromagnetic field build-up and quality factor of electrically large shield enclosures," *IEEE Trans. Electromagn. Compat.*, vol. 40, no. 1, pp. 19–26, Feb. 1998.

Christopher L. Holloway (S'86–M'92–SM'04–F'10) received the B.S. degree from the University of Tennessee at Chattanooga, Chattanooga, in 1986, and the M.S. and Ph.D. degrees from the University of Colorado Boulder, Boulder, in 1988 and 1992, respectively, both in electrical engineering.

During 1992, he was a Research Scientist with Electro Magnetic Applications, Inc., Lakewood, CO. His responsibilities included theoretical analysis and finite-difference time-domain modeling of various electromagnetic problems. From the fall of 1992 to 1994, he was with the National Center for Atmospheric Research (NCAR), Boulder, CO. While at NCAR his duties included wave propagation modeling, signal processing studies, and radar systems design. From 1994 to 2000, he was with the Institute for Telecommunication Sciences at the U.S. Department of Commerce, Boulder, CO., where he was involved in wave propagation studies. Since 2000, he has been with the National Institute of Standards and Technology, Boulder, CO, where he is involved in electromagnetic theory and metrology. He is also the Graduate Faculty at the University of Colorado Boulder. His research interests include electromagnetic field theory, wave propagation, guided wave structures, remote sensing, numerical methods, metamaterials, measurement techniques, and EMC/EMI issues.

Dr. Holloway is a member of the International Union of Radio Science (URSI) Commissions A, B. He is currently serving as the Chair for U.S. Commission A of the URSI and is an Associate Editor for the IEEE TRANSACTIONS ON ELECTROMAGNETIC COMPATIBILITY. He was the Chairman for the Technical Committee on Computational Electromagnetics (TC-9) of the IEEE Electromagnetic Compatibility (EMC) Society from 2000 to 2005, served as a Co-Chair for the Technical Committee on Nano-Technology and Advanced Materials (TC-11) of the IEEE EMC Society from 2006 to 2011, and served as an IEEE Distinguished Lecturer for the EMC Society from 2004 to 2006.

Haider A. Shah was born in Peshawar, Pakistan, in 1985. He received the B.S. degree in electrical engineering from COMSATS Institute of Information Technology, Islamabad, Pakistan, in 2007, and the M.S. degree in electrical engineering (telecommunication) from the Chalmers University of Technology, Gothenburg, Sweden, in 2010.

From June 2007 to July 2008, he was with Nokia Siemens Networks and a Base Station Sub-System Engineer. He was as a Guest Researcher at the National Institute of Standards and Technology, Boulder, CO. He is currently with Ericsson AB, Sweden, as a Radio Performance Testing Engineer. His research interest includes wireless communication and signal processing.

Ryan J. Pirkl (S'06–M'10) received the B.S., M.S., and Ph.D. degrees in electrical engineering from the Georgia Institute of Technology, Atlanta, in 2005, 2007, and 2010, respectively. For his graduate research, he developed hardware, measurement procedures, and processing tools for *in situ* characterization of radio wave propagation mechanisms.

In 2010, he joined the National Institute of Standards and Technology, Boulder, CO under a National Research Council Postdoctoral Research Associateship. He is currently investigating how reverberation chambers may be used as tunable wireless channel emulators for wireless device testing. His research interests include reverberation chambers, radio wave propagation, and analytical electromagnetics.

Kate A. Remley (S'92–M'99–SM'06) was born in Ann Arbor, MI. She received the Ph.D. degree in electrical and computer engineering from Oregon State University, Corvallis, in 1999.

From 1983 to 1992, she was a Broadcast Engineer in Eugene, OR, serving as a Chief Engineer of an AM/FM broadcast station from 1989 to 1991. Since 1999, she has been with the Electromagnetics Division of the National Institute of Standards and Technology (NIST), Boulder, CO, as an Electronics Engineer. Her research interests at NIST include metrology for wireless systems, characterizing the link between nonlinear circuits and system performance, and developing methods for improved radio communications for the public-safety community.

Dr. Remley was the recipient of the Department of Commerce Bronze and Silver Medals, an ARFTG Best Paper Award, and is a member of the Oregon State University Academy of Distinguished Engineers. She was the Editor-in-Chief of IEEE Microwave Magazine from 2009 to 2011 and was the Chair of the MTT-11 Technical Committee on Microwave Measurements from 2008 to 2010.

David A. Hill (M'72–SM'76–F'87–LF'08) was born in Cleveland, OH, on April 21, 1942. He received the B.S.E.E. and M.S.E.E. degrees from Ohio University, Athens, in 1964 and 1966, respectively, and the Ph.D. degree in electrical engineering from Ohio State University, Columbus, in 1970.

From 1970 to 1971, he was a Visiting Fellow with the Cooperative Institute for Research in Environmental Sciences, Boulder, CO, where he was involved in pulse propagation. From 1971 to 1982, he was with the Institute for Telecommunications Sciences, Boulder, CO, where he was involved in antennas and propagation. Since 1982, he has been with the National Institute of Standards and Technology, Boulder, CO, where he is involved in electromagnetic theory. He is also a Professor Adjoint in the Department of Electrical and Computer Engineering of the University of Colorado, Boulder.

Dr. Hill is a member of the International Union of Radio Science Commissions A, B, E, and F. He has served as a Technical Editor for the IEEE TRANSACTIONS ON GEOSCIENCE AND REMOTE SENSING and the IEEE TRANSACTIONS ON ANTENNAS AND PROPAGATION.

John Ladbury (M'09) was born Denver, CO, 1965. He received the B.S.E.E. and M.S.E.E. degrees (specializing in signal processing) from the University of Colorado, Boulder, in 1987 and 1992, respectively.

Since 1987, he has been involved in EMC metrology in the Radio Frequency Technology Division of National Institute of Standards and Technology in Boulder, CO. His principal focus has been on reverberation chambers, with some investigations into other EMC-related topics such as time-domain measurements and probe calibrations.

Mr. Ladbury is a member of the International Electrotechnical Commission (IEC) joint task force on reverberation chambers. He has received three "best paper" awards at IEEE International EMC symposia over the last six years.